Journal of The Electrochemical Society

Degradation Diagnostics for $Li_4Ti_5O_{12}$-Based Lithium Ion Capacitors: Insights from a Physics-Based Model

Journal of The Electrochemical Society, 2020 **167** 043503

Degradation Diagnostics for $Li_4Ti_5O_{12}$-Based Lithium Ion Capacitors: Insights from a Physics-Based Model

Ganesh Madabattula,[1,*] Billy Wu,[2] Monica Marinescu,[1] and Gregory Offer[1,*,z]

[1]*Department of Mechanical Engineering, Imperial College London, United Kingdom*
[2]*Dyson School of Design Engineering, Imperial College London, United Kingdom*

Lithium ion capacitors are an important energy storage technology, providing the optimum combination of power, energy and cycle life for high power applications. However, there has been minimal work on understanding how they degrade and how this should influence their design. In this work, a 1D electrochemical model of a lithium ion capacitor with activated carbon (AC) as the positive electrode and lithium titanium oxide (LTO) as the negative electrode is used to simulate the consequences of different degradation mechanisms in order to explore how the capacity ratio of the two electrodes affects degradation. The model is used to identify and differentiate capacity loss due to loss of active material (LAM) in the lithiated and de-lithiated state and loss of lithium inventory (LLI). The model shows that, with lower capacity ratios (AC/LTO), LAM in the de-lithiated state cannot be identified as the excess LTO in the cell balances the capacity loss. Cells with balanced electrode capacity ratios are therefore necessary to differentiate LAM in lithiated and de-lithiated states and LLI from each other. We also propose in situ diagnostic techniques which will be useful to optimize a LIC's design. The model, built in COMSOL, is available online.

 [DOI: 10.1149/1945-7111/ab7655]

Manuscript submitted September 30, 2019; revised manuscript received February 4, 2020. Published February 26, 2020.

List of symbols

$a_{i,AC}$	Inter-facial surface area of AC electrode, $m^2\,m^{-3}$
$a_{i,LTO}$	Inter-facial surface area of LTO electrode, $m^2\,m^{-3}$
A_{cell}	Projected cross sectional area of electrode, m^2
c_l	Concentration of electrolyte, mol m^{-3}, subscript:0-initial, f-final
c_s	Concentration of Li in LTO electrode, mol m^{-3}
C_{dl}	Double layer capacitance of AC electrode, $F\,m^{-2}$
D_s	Diffusivity of Li ion in LTO particle, $m^2\,s^{-1}$
D_{eff}	Effective diffusivity of electrolyte in porous electrode, $m^2\,s^{-1}$
$E_{eq,LTO}$	Equilibrium potential of LTO electrode as a function of SOC
$E_{eq,AC,0}$	Equilibrium potential of AC electrode at 0% SOC_{AC}
f	Activity coefficient of electrolyte
i_{1C}	Current density at 1 C rate based on LTO, $A\,m^{-2}$
I_{cell}	Applied cell current density, $A\,m^{-2}$
k_c, k_a	Cathodic and anodic rate constants, $m\,s^{-1}$
L_{AC}	Thickness of AC electrode, m
L_{LTO}	Thickness of LTO electrode, m
L_{sep}	Thickness of separator, m
L_{cc}	Thickness of current collector, m
L_{ref}	Position of reference electrode in a separator from AC electrode, m
Q_{cell}	Cell capacity, C
Q_{AC}	Capacity of AC electrode, C
Q_{LTO}	Capacity of LTO electrode, C
r_P	Radius of LTO particle, m
t	Time, s
t_+	Transference number of cation
T	Temperature, K
V_{cell}	Cell voltage, V
x	Position, m

Greek symbols

α_a, α_c	Transfer coefficients of anodic and cathodic Li intercalation at LTO electrode
ε	Porosity, subscripts: l–liquid phase, s–solid phase, sep–-separator
η	Over-potential for reaction at LTO, V
κ	Electrolyte conductivity, $S\,m^{-1}$, subscript: eff-effective in porous phase
σ	Conductivity of material, i, $S\,m^{-1}$, subscript: eff-effective in porous phase
ϕ_s	Electrode potential, V
ϕ_l	Electrolyte potential, V

Constants

F	Faraday constant, 96,485 $C\,mol^{-1}$
R	Gas constant, 8.314 $Jmol^{-1}K^{-1}$

Lithium ion capacitors (LICs) are an energy storage technology with optimum energy density, power density and longer cycle life for high power applications.[1] They store energy mainly via an electrochemical double layer at the positive electrode and chemical intercalation at the negative electrode.[1–3] One combination of the materials for LICs is activated carbon (AC) as the positive electrode and lithium titanium oxide ($Li_4Ti_5O_{12}$ or LTO) as the negative electrode. Figure 1a shows a schematic of the LIC with AC and LTO electrodes. A common electrolyte used is lithium hexafluorophosphate ($LiPF_6$) salt in a mixture of organic solvents (typically 1 M, EC:DMC).[4,5]

Equations 1 and 2 describe the way charge is stored at the AC and LTO electrodes. At the AC positive electrode, charge is stored via double layer formation by PF_6^- ions and at the LTO negative electrode, charge is stored via Li^+ intercalation reaction:[6]

At positive electrode

$$AC + PF_6^- \underset{\text{disch}}{\overset{\text{ch}}{\rightleftharpoons}} AC^+ \cdot PF_6^- \text{ (double layer)} + e^- \qquad [1]$$

At negative electrode

$$Li_4Ti_5O_{12} + 3Li^+ + 3e^- \underset{\text{disch}}{\overset{\text{ch}}{\rightleftharpoons}} Li_7Ti_5O_{12}. \qquad [2]$$

Figure 1b shows the change in the potentials of the AC and LTO electrodes during charging of a cell from 0 to 2.8 V. The potential of the AC electrode increases from 3.05 to 4.3 V vs Li/Li^+.[4] Below 4.3 V vs Li/Li^+, side reactions due to electrolyte degradation (1 M

*Electrochemical Society Member.
[z]E-mail: gregory.offer@imperial.ac.uk

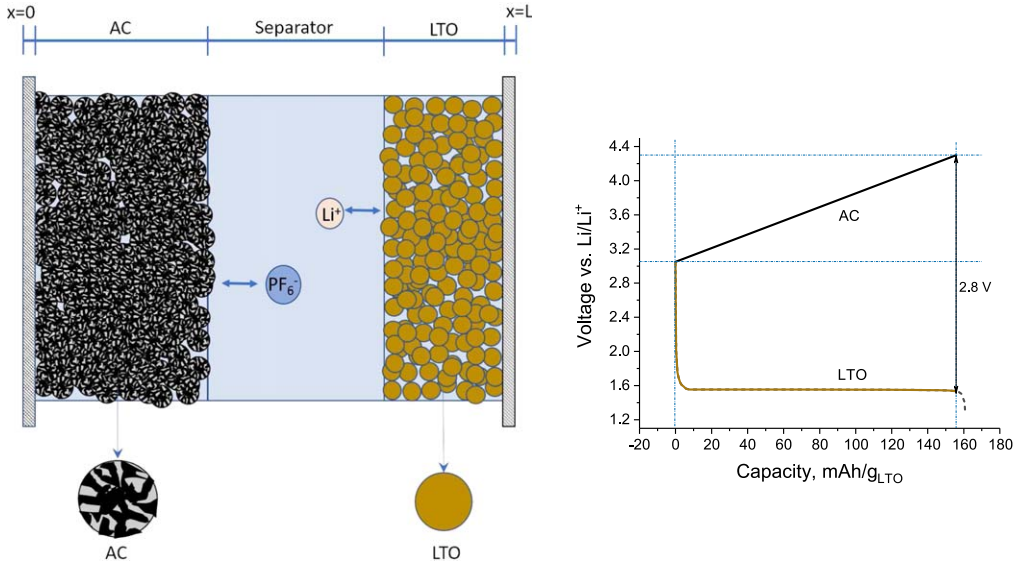

Figure 1. (a) Schematic of a LIC with AC as the positive porous electrode, LTO as the negative porous electrode and 1 M $LiPF_6$ as the electrolyte filling the pores of electrodes and separator. The sizes of the particles and ions are not drawn to scale. (b) A schematic of potential evolution in the AC and LTO electrodes w.r.t. Li/Li^+ during charging of a LIC from 0–2.8 V.[4]

$LiPF_6$ in 1:1 EC:DMC) at the AC electrode are negligible.[4] During charging, $Li_4Ti_5O_{12}$ (spinel) changes its phase to $Li_7Ti_5O_{12}$ (rock salt)[7] and operates at around 1.55 V vs Li/Li^+ for a wide state-of-charge (SOC) range (7%–97.5%)[4] indicating the co-existence of the two phases in this range.[2,4,6,8] However, the LTO electrode undergoes large potential changes when operated close to 0 or 100% SOC i.e. outside the two-phase region. Therefore, it is best to operate a LIC between 7 and 97.5% SOC with respect to the LTO electrode. The theoretical specific capacity of LTO is 175 mAh g^{-1},[9] however the realisable specific capacity achieved in the experiments is around 160 mAh g^{-1}.[4]

LICs achieve higher power densities than lithium-ion batteries by replacing a positive electrode relying upon intercalation with an electrode storing energy in the electrochemical double layer alone, such as AC. An AC electrode can also help LICs achieve longer cycle life due to the absence of the usual degradation mechanisms associated with intercalation, such as those induced by stress and strain. LTO for the negative electrode is also a good choice because it is considered to be a zero-strain material[10–13] and operates well above the electrolyte reduction potential (0.7 V vs Li/Li^+) meaning there is no solid electrolyte interphase (SEI).[9] It also offers better thermal stability.[14] Together this system of electrodes can achieve longer cycle life, higher coulombic efficiency and improved safety.

The mass ratio of the electrodes plays an important role on the power performance of LICs. For specific capacities of 160 mAh g^{-1} and 38.36 mAh g^{-1} for LTO and AC respectively,[4] balancing capacities would require a mass ratio of 4.17. However, for better power performance excess LTO, rather than balancing the capacities of the two electrodes, is beneficial[4,5,15] as the kinetics of LTO are slower than double layer formation.[14] In addition, pre-lithiation of LTO electrode was found to improve capacity retention of cells with cycling.[5] The pre-lithiation also helped increase the capacity of LIC[16] by using the negative-polarization region of the activated carbon.[15] In our previous study,[15] we developed a 1D electrochemical model for a LIC and used it to analyze the effect of mass ratio of the electrodes for optimum LIC design and advantages and disadvantages of pre-lithiation.

The cycling data of LTO based LICs indicates that LICs undergo capacity fade.[1,4–6] Dsoke et al.[4] carried out experiments on LICs at three different mass ratios of the electrodes (AC/LTO) and reported that the capacity retention after 1000 cycles at 10 C was 69.4%, 20.8% and 14.2% for mass ratios of 0.72, 1.54 and 4.17 respectively. The authors, using impedance measurements, reported an increase in the charge transfer resistance after cycling for the three mass ratios; which was higher for higher mass ratio. The authors attributed the loss to the AC electrode. Other experiments by Rauhala et al.[5] on a LIC with AC and LTO electrodes at a mass ratio of 2.5 operated within the flat voltage range of the LTO electrode resulted in 99.8% coulombic efficiency during 1000 cycles at 5 C with 92.2% energy retention. In neither study was the detailed mechanism for degradation discussed.

Gassing, such as of H_2, CO_2 and CO, is a concern in LTO containing pouch cell lithium ion batteries (LIBs).[9,11,14,17] He et al.[9] reported that gas generation at the LTO electrode is due to an intrinsic reaction between LTO and electrolyte at the interface. The authors reported that the reaction is much slower than the electrolyte reduction which occurs below 0.7 V vs Li/Li^+ and leads to slower formation of SEI layer and gassing even above 1.0 V vs Li/Li^+.[9,12] Due to the slower reaction, the SEI formation on LTO occurs over several cycles of charge/discharge and long term storage and leads to long term capacity fade.[9] The gassing continues till SEI formation is complete.[9] Though not reported yet, the same gassing mechanism may also be one of the reasons for capacity fade in LTO-based LICs.

In this work, we use a previously developed 1D electrochemical model[15] to explore the consequences of different degradation modes in order to help interpret previously published[4] experimental data. In LIBs, degradation mechanisms can be classified as loss of active material (LAM) in the lithiated and de-lithiated state or loss of lithium inventory (LLI).[18] Similarly, we classify the degradation in LICs as occurring due to LAM and LLI. The model predicts the voltage profiles of the electrodes of degraded LICs at low currents and we have used it to propose some simple in-situ diagnostic techniques for these degradation mechanisms. In this initial work, thermal effects[11] on degradation are ignored.

Diagnostics for LAM and LLI

In this section, we introduce how capacity fade in LICs affects voltage vs capacity profiles of the electrodes for different degradation mechanisms. The changes in the voltage profiles when compared to the profiles at beginning-of-life help diagnose the degradation mechanisms. These techniques can be applied at low currents and do not account for IR losses as a result of degradation.

The reasons for capacity and power fade due to LAM and LLI in LIBs are described below:[18–20]

i. LAM: the electrode active material is no longer available for Li insertion due to particle cracking, loss of electrical contact, or blocking of active sites by resistive layers formed due to side reactions. It can further be classified as LAM in delithiated or uncharged electrode (LAM_{de}) and LAM in lithiated or charged electrode (LAM_{li}).
ii. LLI: the inserted Li is consumed by parasitic reactions such as SEI growth, Li plating, decomposition reactions. The resistive layers formed due to decomposition reactions cause power fade.

As mentioned before, we classify the degradation in LICs as LAM_{de}, LAM_{li} and LLI, in-line with the literature[18–20] on degradation in LIBs. In this work we have attributed all of the degradation to the negative LTO electrode as the double layer capacitor electrodes are known to offer higher cycle life (10^5–10^6) with higher power density and lower mechanical stresses.[21,22] This assumption is tested in Results and Discussion section.

Figure 2 illustrates the effect of these three degradation modes (LAM_{de}, LAM_{li} and LLI) on an AC/LTO LIC cell with a capacity balanced mass ratio of 4.17, further referred to as "LIC417" in both the discharged and charged states. The figure also illustrates the working of the cell at beginning-of-life (BOL) for comparison. The area of the electrode blocks is proportional to the mass ratio of the electrodes. The light yellow color represents the uncharged LTO ($Li_4Ti_5O_{12}$). The light gray color represents the uncharged AC. Similarly, the dark yellow and dark gray color represent the charged LTO ($Li_7Ti_5O_{12}$) and charged AC respectively. The lighter and darker blue color blocks represent the depleted and no-depleted electrolyte. The voltage vs capacity profiles at low currents for each case are also shown on the right. These profiles are obtained using the equilibrium charging data[4] of LTO at 1 C with 160 mAh g^{-1} and the double layer capacitance of AC as ~110 F g^{-1}. The effect of IR losses on these profiles can be ignored at such low currents. It is assumed that sufficient volume of electrolyte is maintained in the device such that the average electrolyte concentration does not drop below 0.6 M on complete charge to maintain good ionic conductivity.[15]

For an initial concentration of c_{l0}, a cell capacity of Q_{cell} and an averaged concentration of c_{lf} at end-of-charge (EOC), the volume of electrolyte (V_x) required in the pores of electrodes and separator is given by

$$V_x = \frac{Q_{cell}}{F(c_{l0} - c_{lf})} \quad [3]$$

where F is Faraday constant. For $c_{l0} = 1$ M, $c_{lf} = 0.6$ M and $Q_{cell} = 38.36$ mAh g^{-1} of AC, we require $V_x = 3.58$ ml (Eq. 3) of 1 M electrolyte per gram of AC for mass ratios ⩽4.17. At BOL, if LIC417 is charged to 97.5% SOC, the drop in concentration will be to 0.61 M ($c_{l0} - 0.975 \times (c_{l0} - c_{lf})$).

Beginning-of-life.—Figure 2a illustrates the charging of LIC417 at BOL. The left one represents an uncharged LIC, the middle one represents a charged one when the LIC is charged to the maximum SOC limit of LTO i.e. 97.5% ($0.975 \times 160 = 156$ mAh) The cell capacity is limited by both the electrodes. The average electrolyte concentration drops to 0.61 M. The AC electrode is charged upto ~4.3 V (4.27 V) and the cross-patterned area in the voltage vs capacity figure indicates the net available energy.

LAM_{de}.—Figure 2b illustrates the case of 30% loss of delithiated active material from the LTO electrode (LAM_{de}). The left one represents an uncharged LIC, the middle one represents a charged one when the LIC is charged to the maximum SOC limit of LTO i.e. 97.5% ($0.975 \times 0.7 \times 160 = 109$ mAh). The inclined patterned yellow block represents the loss of 30% uncharged LTO due to LAM_{de} which is no longer available for Li insertion. It causes the LTO capacity of the LIC to shrink from 160 to 112 mAh. In this case, the cell capacity is limited by the capacity of the LTO electrode and the effective mass ratio becomes 5.96. Such mass ratio which is above the balanced capacity ratio (4.17) leads to poor performance due to slower kinetics of LTO.[5,15] In this mode, when the device is charged, the AC electrode is under-utilized (UU) at the higher potential ranges, limiting the potential to 3.92 V ($3.05 + 0.7 \times (4.3 - 3.05)$) and the SOC_{AC} to ~68.3% (0.7×0.975). This UU of the AC at higher potential values is a sign of LAM_{de} and helps to quantify the loss when compared to the voltage profile at BOL. During charge, the average concentration of electrolyte drops to 0.73 M ($c_{l0} - 0.975 \times 0.7 \times (c_{l0} - c_{lf})$) instead of 0.61 M in the cell. The cross-patterned area in the voltage vs capacity figure indicates the reduced available energy which can be compared with the BOL's shown in Fig. 2a.

LAM_{li}.—Figure 2c shows the schematics of LIC417 with 30% LAM_{li} in LTO electrode with 97.5% SOC. The left one represents the charged LIC and the middle one represents the discharged LIC. The inclined patterned block with both lithiated (97.5%) and unlithiated (2.5%) LTO represents 30% LAM_{li} in LTO electrode and the inserted Li in it becomes no longer available for discharge. In this case, the LTO electrode becomes limiting, and the AC electrode is under-utilized (UU) at lower potential ranges. The affected LTO profile with 30% LAM_{li} is shown on the right. The profile shrinks on the x-axis by 30% while the SOC is maintained at 97.5%. On discharge, the AC electrode drops to 29.3% SOC (0.3×0.975) and 3.43 V ($3.05 + 0.3 \times (4.3 - 3.05)$) and the remaining charge is unavailable for utilization. The net accessible capacity of the LIC thus is 109 mAh. The affected AC electrode voltage profile with UU at lower potential ranges is a sign of LAM_{li} and helps to quantify the loss when compared to the BOL's profile. During discharge, the average concentration of the electrolyte rises to 0.88 M ($c_{l0} - 0.975 \times 0.3 \times (c_{l0} - c_{lf})$) instead of 1.0 M in the cell. The reduced energy available is represented by the cross-patterned area in the voltage vs capacity profile. We assumed self-discharge and other possible side reactions at the AC electrode are negligible; if this were not the case, the un-utilized charge would be consumed with time.

It is worth noting that when cycling while or after incurring LAM_{de} and LAM_{li}, maintaining the same cell current would cause the local current density to increase, which would most likely accelerate degradation in the subsequent cycles.[18]

LLI.—Figure 2d shows the schematics of a LIC417 with 30% LLI in the LTO electrode. The inclined patterned brown color block represents 30% LLI, which is taken out from the charged LTO (initially at 97.5% SOC) and no longer available for discharge. For a cell in this state, the charge lost to LLI would most likely have been consumed by side reactions between active Li and electrolyte and might have formed a resistive SEI layer, but this is not considered here. Just considering 30% LLI decreases the SOC in LTO from 97.5% to 68.3% for a charged LIC, and causes the LTO profile to be shifted w.r.t. the AC electrode, but not shrink as caused by LAM. Meanwhile, the charge stored at the AC electrode would remain the same, but LLI causes the AC electrode to be under-utilized at lower voltage range. Again, the affected AC voltage profile with UU at lower voltage ranges is a sign of LLI and helps in quantifying the loss. On discharge, AC potential cannot drop below 3.43 V ($3.05 + 0.3 \times (4.3 - 3.05)$) and 29.3% ($0.3 \times 0.975$) charge in the AC electrode cannot be recovered as the LIC's capacity is limited by LTO electrode. During discharge, similar to LAM_{li}, the average concentration of the electrolyte rises to 0.88 M instead of 1.0 M in the cell.

Degradation at lower mass ratios.—As mass ratio affects degradation,[4] we now look at the degradation mechanisms in a LIC with mass ratio of 1.54, referred to as "LIC154". Now the cell capacity is limited by the AC electrode and the capacity reduces to

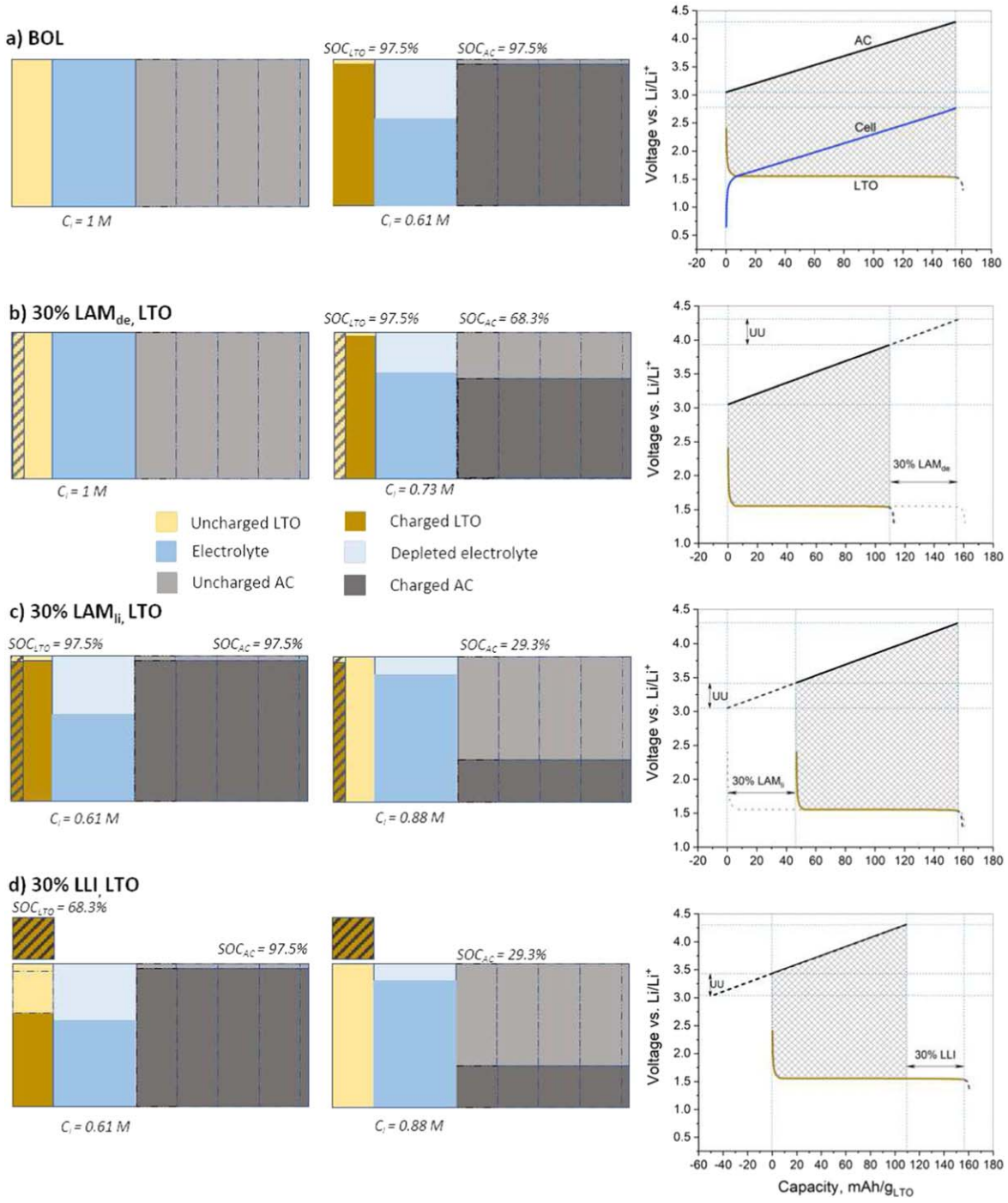

Figure 2. Schematics of a LIC with a 4.17 AC/LTO mass ratio, with different degradation modes. (a) Beginning-of-life (BOL), (b) 30% loss of active material, de-lithiated (LAM_{de}), (c) 30% loss of active material, lithiated (LAM_{li}) and (d) 30% loss of lithium inventory (LLI). The area of the electrodes is proportional to their relative mass. UU:under-utilization. Voltage vs capacity profiles for each mode are also shown. The cross-patterned area in the profiles represents the available energy in each mode.

36.9% of LIC417 (1.54/4.17). Figure 3 illustrates the degradation in LIC154 due to 30% LAM_{de}, 30% LAM_{li} and 30% LLI in LTO electrode. The figure also illustrates the cell at BOL. The respective changes in LTO, AC and the average concentration of electrolyte for each degradation mechanism in charged/discharged LICs are shown in the schematics. The corresponding charge/discharge profile of AC and LTO are also shown. LAM_{li} and LLI have identical consequences to the case of a LIC417. Unlike in LIC417, LAM_{de} in LIC154 does not affect the charge-discharge voltage profiles, nor the achievable energy. This is due to the availability of excess active material of LTO, which mitigates the possible effects of LAM_{de}. Due to this effect, LAM_{de} cannot be detected from the voltage profile in cells with excess LTO, especially if run at low currents; however, an associated increase in cell resistance is expected, which should be visible at high currents. This could be one reason for lower capacity fade in a LIC with lower mass ratio when compared to higher mass ratio as observed by Dsoke et al.[4]

It is assumed that same volume of electrolyte is maintained in LIC154 as in LIC417. Then, at BOL, the drop in electrolyte concentration at EOC is 0.85 M ($c_{l0} - 1 \times 0.369 \times (c_{l0} - c_{lf})$). For 30% LAM_{de}, the drop in electrolyte concentration at EOC is also 0.85 M ($c_{l0} - 1 \times 0.369 \times (c_{l0} - c_{lf})$) and the rise in

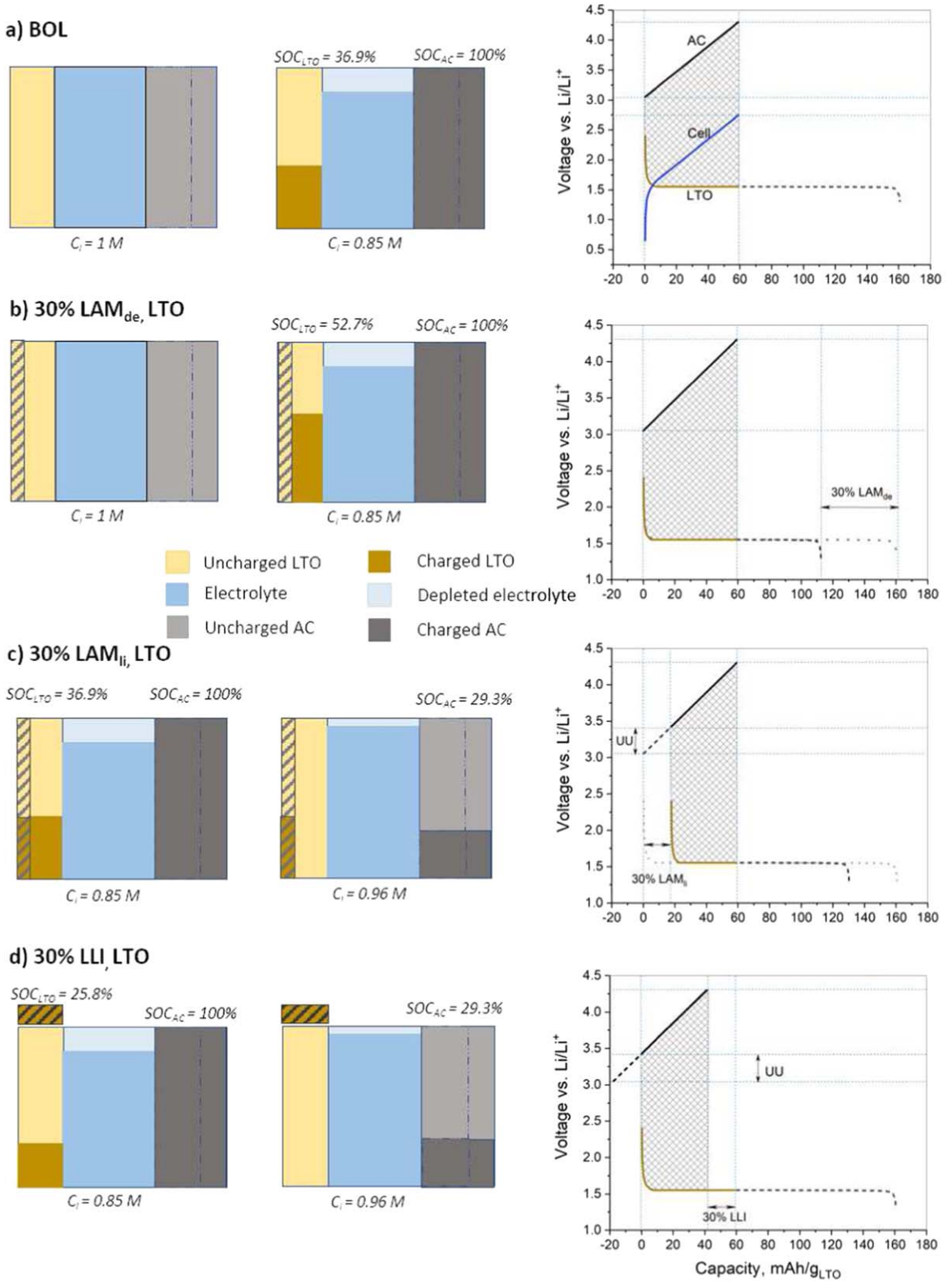

Figure 3. Schematics of a LIC with a 1.54 AC/LTO mass ratio, with different degradation modes. (a) Beginning of life (BOL), (b) 30% loss of active material, de-lithiated (LAM_{de}), (c) 30% loss of active material, lithiated (LAM_{li}) and (d) 30% loss of lithium inventory (LLI). The area of the electrodes is proportional to their relative mass. UU:under-utilization. Voltage vs capacity profiles for each mode are also shown. The cross-patterned area in the profiles represents the available energy in each mode.

SOC_{LTO} is 52.7% (0.369/0.7). For 30% LAM_{li} and 30% LLI, the concentration at the end-of-discharge (EOD) is 0.96 M ($c_{l0} - 0.3 \times 0.369 \times (c_{l0} - c_{lf})$).

The profiles of 30% LAM_{li} and 30% LLI for both the LICs look similar and make it difficult to differentiate one mechanism from the other. Nevertheless, they can be differentiated using over-charging

of LIC417. This aspect using the model will be demonstrated in Results and Discussion section.

LLI with pre-lithiation.—As mentioned before, pre-lithiation of LTO electrode improves the capacity retention of the cell during cycling.[5] The profile (Fig. 3d) for LLI shows that if the active Li in LTO is lost due to LLI, the LTO electrode is forced to undergo large potential changes during discharge (Fig. 3d). Consequently, there is an under-utilization of the AC electrode and the LIC capacity gets negatively affected. In such cases, lost Li due to LLI can be balanced by the Li used for pre-lithiation, resulting in better capacity retention and better utilization of the AC electrode. Figure 4 illustrates this potential advantage of pre-lithiation in LIC154 affected by LLI. Here, UPL represents the utilization of pre-lithiated Li. Thus, the optimization of pre-lithiation level[15] also needs to consider the degradation loss due to LLI.

Precipitation of salt.—During discharge of a LIC, the released ions into electrolyte lead to increase in the local concentration in LTO electrode due to ion diffusion limitations.[6,15] For a $LiPF_6$ electrolyte, if the salt concentration increases beyond 1.5 M, precipitation of $LiPF_6$ salt and significant decrease in conductivity can occur,[23] and, consequently, a decrease in capacity and increase in resistance. In the voltage range of 1.5–4.3 V vs Li/Li^+ in a LIC, the salt precipitation effects can also explain the capacity fade during cycling. Stewart et al.[6] suggested that increasing LTO electrode thickness, equivalent to a decrease in AC:LTO mass ratio, may mitigate the negative effects of electrolyte precipitation on the capacity and power of the cell. The precipitation effects are cumulative with cycle number and higher for the higher mass ratio.[15]

Precipitated salt could dissolve back into the electrolyte partly or fully due to the concentration gradient, leading to partial or full capacity recovery. This can be verified by leaving the LIC cell at open-circuit, and the capacity checked after different durations, expecting higher capacities the longer the cell has rested. The capacity can be measured at a low current before and after relaxation, to avoid confusion between dissolution-caused capacity recovery and that caused by charge-redistribution[24] due to the porous electrode effect.

In reality, capacity fade can be caused by a combination of the mechanisms discussed above. The model proposed in our previous work[15] would serve as an ideal platform to help better understand the effects of multiple, coupled degradation mechanisms in LICs, by testing the effects of a variety of degradation scenarios. The effect of varying mass ratio, LAM and LLI on LIC performance at low currents are discussed next using the model.

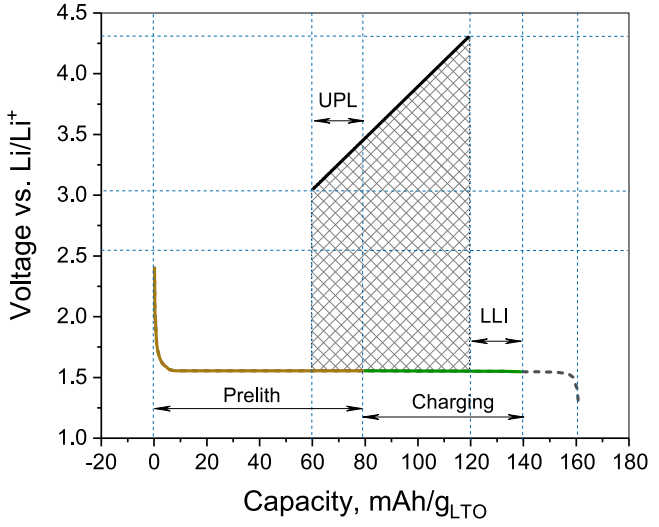

Figure 4. Effect of pre-lithiation on loss of lithium inventory (LLI) in a LIC with a 1.54 AC/LTO mass ratio. The cell is pre-lithiated to 50%, as represented by *Prelith*, before charging. The loss of charge due to LLI is balanced by utilizing the pre-lithiated Li (UPL).

Modelling and Simulation Details

The 1D electrochemical model for a LIC based on Newman's porous electrode theory[6,24–27] was taken from our previous work.[15,28] The model solves for potentials of the electrodes (ϕ_s) and the electrolyte (ϕ_l), the concentration of electrolyte (c_l) and the concentration of Li-ion in LTO particle (c_s), four variables in total. The 1D model geometry is represented in the schematic in Fig. 1a. The model was parameterised based on the data reported by Dsoke et al.[4] at 1 C for the LIC417 and validated in our previous work.[15] The model equations, parameters, initial conditions and boundary conditions for the simulations are given in Appendix.

The model doesn't include any term for degradation. Instead, in this work, the model was simulated to predict the consequences of degradation due to LAM_{de}, LAM_{li} and LLI on voltage vs time profile by changing the parameters. For LAM_{de}, the thickness of LTO electrode was reduced and the initial conditions represent an uncharged cell. For LAM_{li}, the initial conditions of the cell had been changed to represent a charged cell and then the thickness of LTO was reduced. For LLI, the initial conditions of the cell had been changed to represent a charged state and then SOC of the LTO alone was reduced from the charged state. The changes in parameters for each case are represented in Table I. The remaining parameters are given in Table III in Appendix.

The model was solved in COMSOL Multiphysics (v. 5.3a) with Lithium-ion battery module, and was run on a HP platform with Xeon(R) processors, 64 GB RAM, and Windows 10 operating system. "Direct(PARDISO)" solver with a relative tolerance of 10^{-5} was used. The maximum element size was 1×10^{-7} m. The refinement option in AC and LTO domains was applied. The convergence was verified by varying the mesh size and comparing voltage vs time profiles. The time steps taken were controlled by the software. 0.07% SOC of LTO was used to initialize the charge simulations of a LIC at 0% SOC to avoid the numerical errors. A full Fick's law for Li-diffusion in LTO particles at each x-position was solved by COMSOL in the r-direction (radius) with 30 elements. For LAM_{li} and LLI, the cell had been discharged completely first, then the cell was let to cycle using the end of discharge simulation as an initial condition for generating the cycle data. The model file used for the simulations (.mph) built in COMSOL Multiphysics is available at this source[29] under an open-source license.

Results and Discussion

Diagnosing LAM_{de}, LAM_{li} and LLI.—Simulation results for LIC154 and LIC417 with different degradation modes at 1 C are shown in Fig. 5. The cell and electrode potentials of AC and LTO are presented separately for both the cells. For 30% LAM_{de}, the thickness of the LTO was decreased by 30% in the simulations. Similarly, for 30% LAM_{li}, the thickness of the LTO was decreased by 30% and the initial conditions were changed to represent a fully charged state. For 30% LLI, the SOC of LTO was reduced by 30% of that at the fully charged condition without changing the electrode thickness. Model predications for a combination of 10% LAM_{li} and 20% LLI in LIC417 are also shown in Fig. 5. For comparison, model predictions for the cells at BOL are also shown.

Predicted electrode and cell potentials for the LIC154 cell, shown in Figs. 5a and 5b, indicate that LAM_{de} cannot be differentiated from the profiles at BOL as discussed before. The excess LTO in the cell balances the loss. This translates into better cycle life, potentially explaining the observed lower capacity fade in LICs with lower mass ratio.[4] In LAM_{li} and LLI modes, the model predicts under-utilization of the AC electrode at lower values of voltage and the resulting effect on cell potential can also be seen. While they can be identified

Table I. The parameters and the initial conditions used for the degradation simulations at different mass ratios. The remaining parameters are taken from our previous work.[15]

Degradation	LIC417	LIC154	LIC072
BOL	1 C, $L_{LTO} = 20\ \mu$m, $SOC_{AC} = 0$, $Prelith = 0.07\%$, $c_{l0} = 1$ M, t = 3201 s.	1 C, $L_{LTO} = 20\ \mu$m, $SOC_{AC} = 0$, $Prelith = 0.07\%$, $c_{l0} = 1$ M, t = 1250 s.	10 C, $L_{LTO} = 20\ \mu$m, $SOC_{AC} = 0$, $Prelith = 0.07\%$, $c_{l0} = 1$ M, t = 59 s.
30% LAM_{de}	1 C, $L_{LTO} = 14\ \mu$m, $SOC_{AC} = 0$, $Prelith = 0.07\%$, $c_{l0} = 1$ M, t = 2310 s.	1 C, $L_{LTO} = 14\ \mu$m, $SOC_{AC} = 0$, $Prelith = 0.07\%$, $c_{l0} = 1$ M, t = 1250 s.	—
30% LAM_{li}	1 C, $L_{LTO} = 14\ \mu$m, $SOC_{AC} = 94.3\%$, $Prelith = 0\%$, $c_{l0} = 0.572$ M, t = 2247 s, overcharge: t = 2288 s.	1 C, $L_{LTO} = 14\ \mu$m, $SOC_{AC} = 100\%$, $Prelith = 0\%$, $c_{l0} = 0.624$ M, t = 875 s.	10 C, $L_{LTO} = 14\ \mu$m, $SOC_{AC} = 100\%$, $Prelith = 0\%$, $c_{l0} = 0.629$ M, t = 43 s.
30% LLI	1 C, $L_{LTO} = 20\ \mu$m, $SOC_{AC} = 94.3\%$, $SOC_{LTO} = 68.28\%$, $Prelith = 0\%$, $c_{l0} = 0.572$ M, t = 2247 s, overcharge: t = 2802 s.	1 C, $L_{LTO} = 20\ \mu$m, $SOC_{AC} = 100\%$, $SOC_{LTO} = 26.6\%$, $Prelith = 0\%$, $c_{l0} = 0.624$ M, t = 875 s.	10 C, $L_{LTO} = 20\ \mu$m, $SOC_{AC} = 100\%$, $SOC_{LTO} = 13.29\%$, $Prelith = 0\%$, $c_{l0} = 0.629$ M, t = 43 s.
10% LAM_{li} + 20% LLI	1 C, $L_{LTO} = 18\ \mu$m, $SOC_{AC} = 94.3\%$, $SOC_{LTO} = 78\%$, $Prelith = 0\%$, $c_{l0} = 0.572$ M, t = 2310 s, overcharge: t = 2810 s.	—	—

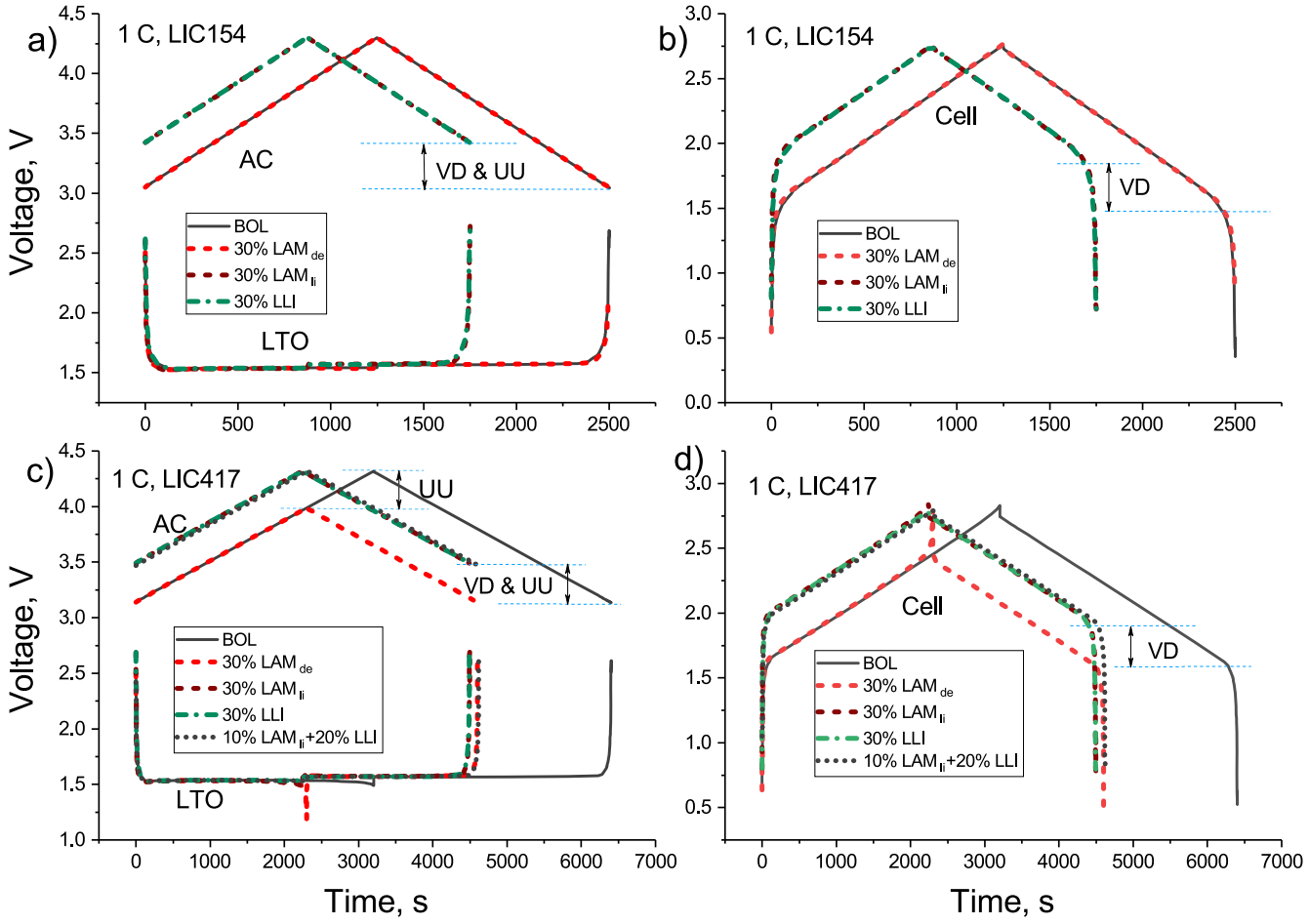

Figure 5. Model predictions of cell and electrode potentials of LIC154 and LIC417 with different degradation mechanisms at 1 C: 30% LAM_{de}, 30% LAM_{li}, 30% LLI and 10% LAM_{li} + 20% LLI. (a) AC and LTO electrodes, LIC154, (b) cell, LIC154, (c) AC and LTO electrode, LIC417 and (c) cell, LIC417. The simulations show that it is difficult to differentiate 30% LAM_{li} from 30% LLI in both the cell. BOL: beginning-of-life.

using voltage drift (VD) and under-utilization (UU) of AC electrode, the profiles of electrodes and cell of LAM_{li} and LLI appear identical during charge and discharge and cannot be distinguished from each other. This inability to distinguish LAM_{li} and LLI and identify LAM_{de} at lower mass ratios makes the case for the need of studying/identifying the degradation mechanisms using LIC417 irrespective of its cycle life.

The simulations for LIC417 shown in Figs. 5c and 5d indicate that LAM_{de} can be identified in LIC417 with the help of difference in the profiles of electrodes and cell during charge-discharge from the BOL profiles. The AC voltage profile shows under-utilization at higher values of the electrode potential. The LTO voltage profile shows a spike during charging, around 2.8 V cell voltage (Fig. 5c), unlike for LIC154, which would generate a sharp increase of cell voltage at the end of the charge (Fig. 5d). These can be the signs of LAM_{de}. In normal charging conditions, the profiles for LAM_{li}, LLI and the combination of LAM_{li} and LLI do not look different.

In order to distinguish LAM_{li} from LLI, overcharging was simulated, by charging the cell to 3.0 V instead of 2.8 V for all three degradation cases. Predicted electrode and cell potentials for LIC417 are shown in Fig. 6. The results show that LAM_{li} can be differentiated from LLI and the combination of LLI and LAM_{li} using the spike from the LTO electrode. However, care has to be taken to separate the changes due to side-reactions at the AC electrode above 2.8 V cell potential, which we did not include in the model, from the changes caused by 30% LAM_{li}. The measurement of the AC electrode potential above 2.8 V at BOL would make it easier for the diagnosis. The 10% LAM_{li} in the combined degradation test is dominated by the 20% LLI and similar to that for sole 30% LLI degradation. One can conclude that if LTO is in excess, separating LAM_{li} from LLI might not be possible from voltage profiles.

Regardless, the model predicts under-utilization and voltage drift in the three degradation mechanisms and demonstrates its ability to quantify the capacity loss. When seen together with the spike in LTO voltage profiles, the model identifies the mechanisms in LIC417. The predictions for 30% LAM_{de} show under-utilization of the AC electrode at the higher values of voltage whereas the predictions for 30% LAM_{li} and 30% LLI show under-utilization of AC electrode at the lower values of voltage. The spike in the LTO voltage profile helps in identifying LAM_{de} when charged to normal cutoff voltage and differentiating LAM_{li} from LLI when over-charged to 3.0 V.

Analysis of capacity loss data.—The cycling data of Dsoke et al.[4] at 10 C rate for a LIC with mass ratio of 0.72, referred to as "LIC072" is shown in Fig. 7. The authors compared the electrode potentials of AC and LTO extracted from the 5th and 999th cycles. The data shows four important characteristics of capacity fade in a LIC. First, there is about 30% loss in capacity of the cell by the 999th cycle when compared to the 5th cycle. Second, there is a voltage drift (VD) in the electrode potential of AC w.r.t. the reference electrode and under-utilization of the AC electrode. Third, the change in slope of the AC electrode in both the cycles

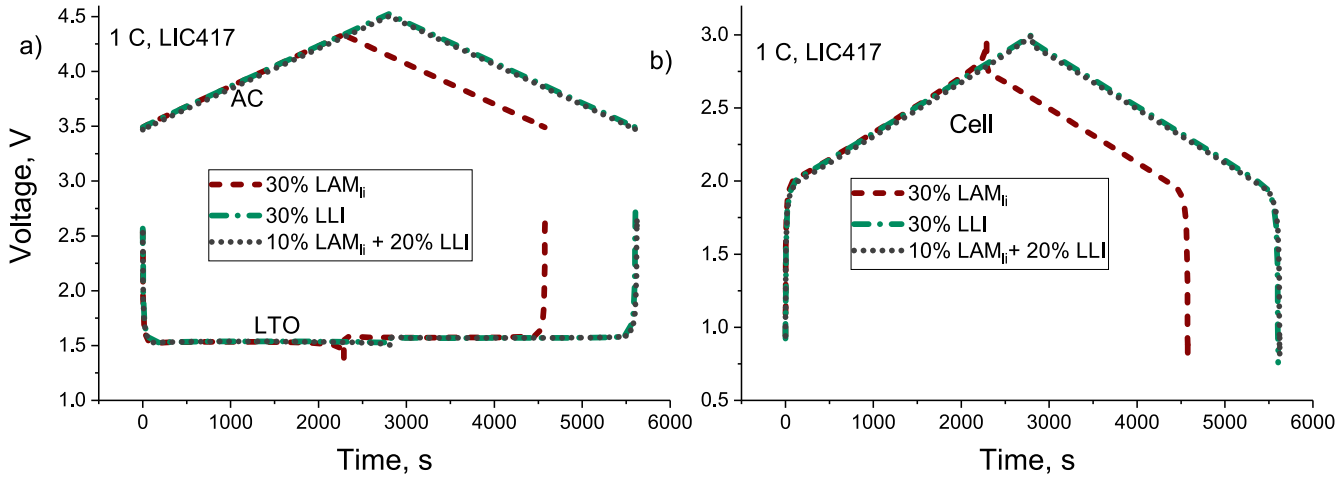

Figure 6. Overcharge simulations of LIC417 to 3.0 V with 30% LAM$_{li}$, 30% LLI and a combination of 10% LAM$_{li}$ and 20% LLI. The simulations show that 30% LAM$_{li}$ can be differentiated from 30% LLI using the spike in LTO electrode when charged above 2.8 V.

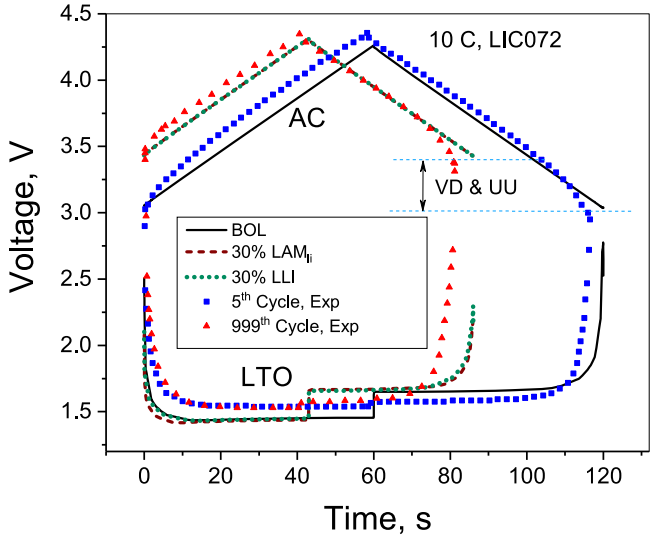

Figure 7. Comparison of simulations with the data of LIC072 at 5th and 999th cycles at 10 C. Experimental data is reproduced from Dsoke et al.[4] The simulations are carried out with 30% LAM$_{li}$ and 30% LLI as sole degradation modes respectively, at LTO for 999th cycle.

is negligible. Fourth, there is an increase in IR drop of the LTO electrode in the 999th cycle when the cell is changed from charge to discharge.

The voltage drift and under-utilization of the AC electrode at lower potentials can be due to LAM$_{li}$ or/and LLI as discussed before . The negligible change in slope of the AC electrode in the 999th cycle compared to 5th cycle indicates that the degradation at AC electrode due to LAM is negligible. Otherwise, a change in slope due to change in capacity should be seen. The increase in IR drop at 10 C can be due to a resistive layer present in the 999th cycle.

The present model can be used to interpret and understand these features observed in Dsoke et al.[4] Model predictions of 30% LAM$_{li}$ and 30% LLI in LIC072 are compared to the experimental data in the figure. Both 30% LAM$_{li}$ and 30% LLI are in agreement with the data, suggesting either one of the mechanisms can be the cause for the observed capacity fade. The increase in IR drop can be attributed to either 30% LAM$_{li}$ or 30% LLI.

On the other hand, the agreement between the data and simulations for both the cycles with the same value of double layer capacitance of AC electrode also confirm that the degradation mechanisms due to LAM at AC are negligible.

Thus, the model can be used to diagnose and quantify the capacity loss due to LAM$_{de}$, LAM$_{li}$ and LLI at low currents where IR losses are minimum. The lack of data for LIC417 limits the present model to diagnose the mechanisms further.

Conclusions

A 1D electrochemical model previously created for beginning of life of lithium ion capacitors[15] is used here to predict the effect of LAM$_{de}$, LAM$_{li}$, LLI and a combination of these modes on electrode and cell voltage profiles at low currents. The model file (.mph) built in COMSOL is available online[29] under open-source license. Using the model predictions, we propose in situ diagnostic techniques for LAM$_{de}$, LAM$_{li}$ and LLI using electrode potential profiles. The model predicts a stark effect of electrode mass ratio on the capacity fade caused by the various degradation mechanisms. Hence, capacity fade in LICs should never be investigated independent from knowledge of the cell design, particularly of the degree of pre-lithiation and the mass ratio of electrodes. At lower mass ratios than those corresponding to a balanced cell, the model predicts that LAM$_{de}$ cannot be identified, as the excess LTO is utilized to balance the capacity loss and extends the cycle life, and LAM$_{li}$ and LLI cannot be differentiated from each other. The model predicts that in a balanced LIC, with electrode mass ratio corresponding to equal capacity of electrodes, LAM$_{de}$, LAM$_{li}$ and LLI can be distinguished from one another, by quantifying the under-utilization and voltage-drift of the AC electrode potential and spikes in LTO potential during cycling. The model suggests that over-charging of the capacity balanced cell helps in differentiating LAM$_{li}$ from LLI, which is otherwise difficult. The drift in the potential of the AC electrode during cycling, observed experimentally,[4] can be interpreted via the model as a result of capacity loss by LAM$_{li}$ or LLI at the LTO electrode, and not due to degradation in the AC electrode.

Acknowledgments

The authors gratefully acknowledge Innovate UK for funding "Advanced Lithium Ion Capacitors and Electrodes (ALICE)–102655" project.

Appendix

A summary of the model equations is given in Table II. Table III lists the parameters. Table IV shows the boundary conditions w.r.t. the spatial dimension, x, and Table V lists SOC-dependent initial values. We used the parameters obtained for the LIC072, LIC154 and LIC417 of Dsoke et al.,[4] which were analysed and found to have cell to cell variation in IR losses and slightly different mass ratios.[15] The LIC072 had a mass ratio of 0.8, the LIC154 had a mass ratio of

Table II. A summary of the model equations for a LIC, taken from our previous work.[15] .

AC and LTO electrodes
Electrode current density: $i_s = -\sigma_{eff}\frac{\partial \phi_s}{\partial x}$
Charge conservation in electrode phase: $\frac{\partial i_s}{\partial x} = -a_i j_s$
Electrolyte current density: $i_l = -\kappa_{eff}\frac{\partial \phi_l}{\partial x} + \frac{2\kappa_{eff}(1-t_+)RT}{F}\left(1+\frac{\partial \ln f}{\partial \ln c_l}\right)\frac{\partial \ln c_l}{\partial x}$
Charge conservation in electrolyte phase: $\frac{\partial i_l}{\partial x} = a_i j_s$
Ionic flux of electrolyte: $N_l = -D_{eff}\frac{\partial c_l}{\partial x} + \frac{i_l t_+}{F}$
Concentration of electrolyte: $\varepsilon_l\frac{\partial c_l}{\partial t} = -\frac{\partial N_l}{\partial x} + \frac{a_i j_s}{F}$
Source term in LTO: $j_{s,-} = i_0\left\{\exp(\frac{\alpha_a F\eta}{RT}) - \exp(\frac{-\alpha_c F\eta}{RT})\right\}$
Exchange current density: $i_0 = F(k_c)^{\alpha_a}(k_a)^{\alpha_c}(c_{s,max}-c_s)^{\alpha_a}(c_s)^{\alpha_c}\left(\frac{c_l}{c_{l,ref}}\right)^{\alpha_a}$
Overpotential: $\eta = \phi_s - \phi_l - E_{eq,LTO}(SOC)$
Source term in AC: $j_{s,+} = C_{dl}\frac{\partial(\phi_s-\phi_l)}{\partial t}$
Concentration of Li in spherical LTO particles: $\frac{\partial c_s}{\partial t} = \frac{1}{r^2}\frac{\partial}{\partial r}\left[r^2 D_s\frac{\partial c_s}{\partial r}\right]$
Separator
Concentration of electrolyte: $\varepsilon_{sep}\frac{\partial c_l}{\partial t} = \frac{\partial}{\partial x}\left[D_{eff,sep}\frac{\partial c_l}{\partial x}\right]$
Electrolyte current density: $i_l = -\kappa_{eff,sep}\frac{\partial \phi_l}{\partial x} + \frac{2\kappa_{eff,sep}(1-t_+)RT}{F}\left(1+\frac{\partial \ln f}{\partial \ln c_l}\right)\frac{\partial \ln c_l}{\partial x}$
Charge conservation in electrolyte phase: $\frac{\partial i_l}{\partial x} = 0$
$\phi_s = 0$ *and* $i_s = 0$
Current Collectors
Current density: $i_s = -\sigma_{Al}\frac{\partial \phi_s}{\partial x}$
Charge conservation: $\frac{\partial i_s}{\partial x} = 0$

1.59 and the LIC417 had a mass ratio of 4.33.[15] The cell to cell variations in IR losses in those cells were fitted using different separator thickness and reference electrode position in each cell.[15] The effective mass ratios were accounted using appropriate AC electrode thickness in the model. These changes affect the initial SOC of electrodes and c_{l0} for the current degradation studies and are different (Table I) from the theoretical values shown in Figs. 2 and 3. However, the conclusions arrived using these values do not change. Concentration dependent properties of 1 M $LiPF_6$ in EC:DEC (1:1) electrolyte at 298.15 K were originally taken from Lundgren et al.[23] and reported in our previous work.[15] E_{eq} of LTO electrode[4] as a function of SOC was also taken from the previous work.[15] It was assumed to be the same during charge and discharge. The effective transport properties of conductivities of the electrodes and electrolyte (σ_{eff}, κ_{eff}) and diffusivity of the electrolyte (D_{eff}) in the porous phase were obtained using Bruggeman correction for tortuosity.[15]

Table III. The list of parameters. The values without references were taken from our previous work.[15]

Parameter	Value
$a_{i,AC}$	9.65×10^6 cm^2 cm^{-3}
$a_{i,LTO}$	11.2×10^4 cm^2 cm^{-3}
α_a, α_c	0.5
A_{cell}	113 mm^2
C_{dl}	6.45×10^{-6} F cm^{-2}
$c_{l,ref}$	1000 mol m^{-3}
$c_{s,max}$	22,852 mol m^{-3} [30]
D_s	6.8×10^{-15} m^2 s^{-1} [31]
δV	1.25 V
$\varepsilon_{l,LTO}$	0.582
$\varepsilon_{l,AC}$	0.717
$\varepsilon_{s,AC}$	0.283
$\varepsilon_{s,LTO}$	0.418
ε_{sep}	0.9
$E_{eq,AC,0}$	3.14 V for LIC417, 3.05 V for LIC154 & LIC072
i_{1C}	0.56 mA cm^{-2}
k_c, k_a	2×10^{-12} m s^{-1}
σ_{AC}	560 S m^{-1} [32]
σ_{LTO}	1.21 S m^{-1} [2]
σ_{Al}	3.55×10^7 S m^{-1} [26]
$L_{AC,072}$	45 μm
$L_{AC,154}$	90 μm
$L_{AC,417}$	245 μm
L_{LTO}	20 μm
$L_{sep,072}$	140 μm
$L_{sep,154}$	229 μm
$L_{sep,417}$	260 μm
$L_{ref,072}$	135 μm
$L_{ref,154}$	203 μm
$L_{ref,417}$	112 μm
L_{cc}	10 μm
r_P	$3\varepsilon_{s,LTO}/a_{i,LTO}$
T	298 K

At $x = 0$ boundary, the sign of applied cell current, I_{cell} in Table IV depends on charge, discharge, and cycling simulations. At $x = L$, ϕ_s was set as zero as a base potential for all the simulations. The individual electrode potentials were measured w.r.t. a reference electrolyte potential probe ($\phi_{l,ref}$) in the separator at L_{ref}.

The potentials of the electrodes were defined w.r.t. Li/Li^+. Through the parameters "*Prelith*" and "*ExsLTO*", the influence of pre-lithiation level of LTO and excess LTO for a given mass ratio on the initial values was introduced respectively. $SOC_{AC,0}$, $SOC_{LTO,0}$ and *Prelith* values should be self-consistent and between 0 and 1 for a given *ExsLTO* (Table V).

Table IV. Boundary conditions for the model.[15]

	x = 0	$L_{cc,+}$	$L_{cc,+} + L_{AC}$	$L_{cc,+} + L_{AC} + L_{sep}$	$L_{cc,+} + L_{AC} + L_{sep} + L_{LTO}$	L
i_l	0	0	$i_{l,left} = i_{l,right}$	$i_{l,left} = i_{l,right}$	0	0
N_l	0	0	$N_{l,left} = N_{l,right}$	$N_{l,left} = N_{l,right}$	0	0
i_s	I_{cell}	$i_{s,left} = i_{s,right}$	0	0	$i_{s,left} = i_{s,right}$	$\phi_s = \phi_{s,LTO}$
ϕ_l			$\phi_{l,left} = \phi_{l,right}$	$\phi_{l,left} = \phi_{l,right}$		
c_l			$c_{l,left} = c_{l,right}$	$c_{l,left} = c_{l,right}$		
c_s			$-\frac{\partial c_s}{\partial r}\Big\|_{r=0} = 0$ and $-D_s\frac{\partial c_s}{\partial r}\Big\|_{r=r_P} = \frac{j_{s,-}}{F}$			

Table V. Initial conditions[15] as a function of SOC, pre-lithiation level (*Prelith*) and excess LTO (*ExsLTO*) for the simulations.

Variable	Value
Q_{LTO}	$C_{\mathrm{s,max}}\varepsilon_{\mathrm{s,LTO}}A_{\mathrm{cell}}L_{\mathrm{LTO}}F$
Q_{AC}	$C_{\mathrm{dl}}a_{\mathrm{i,AC}}A_{\mathrm{cell}}\delta V\ L_{\mathrm{AC}}$
Q_{cell}	$\min(Q_{\mathrm{LTO}},Q_{\mathrm{AC}}\ )$
C_{rate}	Input
ExsLTO	$Q_{\mathrm{LTO}}/Q_{\mathrm{AC}}$
Prelith	Input, 0-unprelithiated cell
$SOC_{\mathrm{AC},0}$	Input, 0–uncharged
$SOC_{\mathrm{LTO},0}$	$Prelith + \frac{SOC_{\mathrm{AC},0}}{ExsLTO}$
$c_{\mathrm{l},0}$	$\mathrm{c_{l,ref}}\frac{Q_{\mathrm{cell}}\times SOC_{\mathrm{AC},0}}{FA_{\mathrm{cell}}(L_{\mathrm{AC}}\varepsilon_{\mathrm{l,AC}}+L_{\mathrm{sep}}\varepsilon_{\mathrm{sep}}+L_{\mathrm{LTO}}\varepsilon_{\mathrm{l,LTO}})}$
$c_{\mathrm{s0,LTO}}$	$(c_{\mathrm{s,max}}\times SOC_{\mathrm{LTO},0})$
$\phi_{\mathrm{s,LTO},0}$	0
$\phi_{\mathrm{l},0}$	$-E_{\mathrm{eq,LTO}}(SOC_{\mathrm{LTO},0})$
$\phi_{\mathrm{s,AC},0}$	$E_{\mathrm{eq,AC},0}+(\delta V\times SOC_{\mathrm{AC},0})+\phi_{\mathrm{l},0}$
I_{cell}	$\pm i_{\mathrm{1C}}.C_{\mathrm{rate}}$

ORCID

Ganesh Madabattula https://orcid.org/0000-0001-7915-0770
Billy Wu https://orcid.org/0000-0003-3963-4900
Monica Marinescu https://orcid.org/0000-0003-1641-3371
Gregory Offer https://orcid.org/0000-0003-1324-8366

References

1. A. Du Pasquier, I. Plitz, S. Menocal, and G. Amatucci, "A comparative study of li-ion battery, supercapacitor and nonaqueous asymmetric hybrid devices for automotive applications." *Journal of Power Sources*, **115**, 171 (2003).
2. H.-G. Jung, N. Venugopal, B. Scrosati, and Y.-K. Sun, "A high energy and power density hybrid supercapacitor based on an advanced carbon-coated li4ti5o12 electrode." *Journal of Power Sources*, **221**, 266 (2013).
3. M. Lu, *Supercapacitors: Materials, Systems, and Applications* (John Wiley & Sons, United States of America) (2013).
4. S. Dsoke, B. Fuchs, E. Gucciardi, and M. Wohlfahrt-Mehrens, "The importance of the electrode mass ratio in a li-ion capacitor based on activated carbon and li4ti5o12." *Journal of Power Sources*, **282**, 385 (2015).
5. T. Rauhala, J. Leis, T. Kallio, and K. Vuorilehto, "Lithium-ion capacitors using carbide-derived carbon as the positive electrode-a comparison of cells with graphite and li4ti5o12 as the negative electrode." *Journal of Power Sources*, **331**, 156 (2016).
6. S. Stewart, P. Albertus, V. Srinivasan, I. Plitz, N. Pereira, G. Amatucci, and J. Newman, "Optimizing the performance of lithium titanate spinel paired with activated carbon or iron phosphate." *J. Electrochem. Soc.*, **155**, A253 (2008).
7. S. Scharner, W. Weppner, and P. Schmid-Beurmann, "Evidence of two-phase formation upon lithium insertion into the li1. 33ti1. 67 o 4 spinel." *J. Electrochem. Soc.*, **146**, 857 (1999).
8. J.-J. Yang, C.-H. Choi, H.-B. Seo, H.-J. Kim, and S.-G. Park, "Voltage characteristics and capacitance balancing for li4ti5o12/activated carbon hybrid capacitors." *Electrochimica Acta*, **86**, 277 (2012).
9. Y.-B. He et al., "Gassing in li 4 ti 5 o 12-based batteries and its remedy." *Sci. Rep.*, **2**, 913 (2012).
10. T. Ohzuku, A. Ueda, and N. Yamamoto, "Zero-strain insertion material of li [li1/3ti5/3] o 4 for rechargeable lithium cells." *J. Electrochem. Soc.*, **142**, 1431 (1995).
11. J. Gao, B. Gong, Q. Zhang, G. Wang, Y. Dai, and W. Fan, "Study of the surface reaction mechanism of li 4 ti 5 o 12 anode for lithium-ion cells." *Ionics*, **21**, 2409 (2015).
12. Y.-B. He, M. Liu, Z.-D. Huang, B. Zhang, Y. Yu, B. Li, F. Kang, and J.-K. Kim, "Effect of solid electrolyte interface, (sei), film on cyclic performance of li4ti5o12 anodes for li ion batteries." *Journal of Power Sources*, **239**, 269 (2013).
13. G. Xu, P. Han, S. Dong, H. Liu, G. Cui, and L. Chen, "Li4ti5o12-based energy conversion and storage systems: status and prospects." *Coordination Chemistry Reviews*, **343**, 139 (2017).
14. T. Yuan, Z. Tan, C. Ma, J. Yang, Z.-F. Ma, and S. Zheng, "Challenges of spinel li4ti5o12 for lithium-ion battery industrial applications." *Adv. Energy Mater.*, **7**, 1601625 (2017).
15. G. Madabattula, B. Wu, M. Marinescu, and G. Offer, "How to design lithium ion capacitors: modelling, mass ratio of electrodes and pre-lithiation." *J. Electrochem. Soc.*, **167**, 013527 (2020).
16. N. Xu, X. Sun, F. Zhao, X. Jin, X. Zhang, K. Wang, K. Huang, and Y. Ma, "The role of pre-lithiation in activated carbon/li4ti5o12 asymmetric capacitors." *Electrochimica Acta*, **236**, 443 (2017).
17. J. Liu, P. Bian, J. Li, W. Ji, H. Hao, and A. Yu, "Gassing behavior of lithium titanate based lithium ion batteries with different types of electrolytes." *Journal of Power Sources*, **286**, 380 (2015).
18. C. R. Birkl, M. R. Roberts, E. McTurk, P. G. Bruce, and D. A. Howey, "Degradation diagnostics for lithium ion cells." *Journal of Power Sources*, **341**, 373 (2017).
19. M. Dubarry, C. Truchot, and B. Y. Liaw, "Synthesize battery degradation modes via a diagnostic and prognostic model." *Journal of Power Sources*, **219**, 204 (2012).
20. A. Devie, M. Dubarry, and B. Y. Liaw, "Overcharge study in li4ti5o12 based lithium-ion pouch cell i. quantitative diagnosis of degradation modes." *J. Electrochem. Soc.*, **162**, A1033 (2015).
21. J. R. Miller and A. F. Burke, "Electrochemical capacitors: challenges and opportunities for real-world applications." *The Electrochemical Society Interface*, **17**, 53 (2008).
22. A. Burke, Z. Liu, and H. Zhao, "Present and future applications of supercapacitors in electric and hybrid vehicles." *Electric Vehicle Conference, (IEVC), 2014 IEEE International* (IEEE, Italy) p. 1 (2014).
23. H. Lundgren, M. Behm, and G. Lindbergh, "Electrochemical characterization and temperature dependency of mass-transport properties of lipf6 in ec: dec." *J. Electrochem. Soc.*, **162**, A413 (2015).
24. G. Madabattula and S. Kumar, "Insights into charge-redistribution in double layer capacitors." *J. Electrochem. Soc.*, **165**, A636 (2018).
25. M. Doyle, T. F. Fuller, and J. Newman, "Modeling of galvanostatic charge and discharge of the lithium/polymer/insertion cell." *J. Electrochem. Soc.*, **140**, 1526 (1993).
26. M. Torchio, L. Magni, R. B. Gopaluni, R. D. Braatz, and D. M. Raimondo, "Lionsimba: a matlab framework based on a finite volume model suitable for li-ion battery design, simulation, and control." *J. Electrochem. Soc.*, **163**, A1192 (2016).
27. J. Newman and K. E. Thomas-Alyea, *Electrochemical Systems* (John Wiley & Sons, United States of America) (2012).
28. G. Madabattula, B. Wu, M. Marinescu, and G. Offer, *1D Electrochemical Model for Lithium Ion Capacitors in Comsol* (2019), 10.5281/zenodo.3569607.
29. G. Madabattula, B. Wu, M. Marinescu, and G. Offer, *1D Electrochemical Model for Degradation Diagnostics of Lithium Ion Capacitors in Comsol* (2020), 10.5281/zenodo.3636185.
30. M. Rashid, A. Sahoo, A. Gupta, and Y. Sharma, "Numerical modelling of transport limitations in lithium titanate anodes." *Electrochimica Acta*, **283**, 313 (2018).
31. Y. H. Rho and K. Kanamura, "Li+ ion diffusion in li4ti5o12 thin film electrode prepared by pvp sol-gel method." *J. Solid State Chem.*, **177**, 2094 (2004).
32. L. Qie, W. Chen, H. Xu, X. Xiong, Y. Jiang, F. Zou, X. Hu, Y. Xin, Z. Zhang, and Y. Huang, "Synthesis of functionalized 3d hierarchical porous carbon for high-performance supercapacitors." *Energy & Environmental Science*, **6**, 2497 (2013).